OXFORD

SOT | Society of Toxicology
www.toxsci.oxfordjournals.org

TOXICOLOGICAL SCIENCES, 148(2), 2015, 567–580

doi: 10.1093/toxsci/kfv206
Advance Access Publication Date: September 16, 2015
Research Article

2,3,7,8-Tetrachlorodibenzo-*p*-Dioxin Alters Lipid Metabolism and Depletes Immune Cell Populations in the Jejunum of C57BL/6 Mice

Kelly A. Fader,[*,†] Rance Nault,[*,†] Dustin A. Ammendolia,[*] Jack R. Harkema,[†,‡] Kurt J. Williams,[‡] Robert B. Crawford,[†,§] Norbert E. Kaminski,[†,§] Dave Potter,[¶] Bonnie Sharratt,[¶] and Timothy R. Zacharewski[*,†,1]

[*]Department of Biochemistry and Molecular Biology, Michigan State University, East Lansing, Michigan 48824; [†]Institute for Integrative Toxicology, Michigan State University, East Lansing, Michigan 48824; [‡]Department of Pathobiology and Diagnostic Investigation, Michigan State University, East Lansing, Michigan 48824; [§]Department of Pharmacology and Toxicology, Michigan State University, East Lansing, Michigan 48824; and [¶]Wellington Laboratories Inc., Guelph, Ontario N1G 3M5, Canada

[1]To whom correspondence should be addressed at Michigan State University, 603 Wilson Road, Room 309, East Lansing, MI 48824-1319. Fax: 517-353-9334. E-mail: tzachare@msu.edu

ABSTRACT

2,3,7,8-Tetrachlorodibenzo-*p*-dioxin (TCDD) is a potent aryl hydrocarbon receptor agonist that elicits dose-dependent hepatic fat accumulation and inflammation that can progress to steatohepatitis. To investigate intestine—liver interactions that contribute to TCDD-elicited steatohepatitis, we examined the dose-dependent effects of TCDD (0.01, 0.03, 0.1, 0.3, 1, 3, 10, or 30 μg/kg) on jejunal epithelial gene expression in C57BL/6 mice orally gavaged every 4 days for 28 days. Agilent 4x44K whole-genome microarray analysis of the jejunal epithelium identified 439 differentially expressed genes (|fold change| $\geq$ 1.5, P1(*t*) $\geq$ 0.999) across 1 or more doses, many related to lipid metabolism and immune system processes. TCDD-elicited differentially expressed genes were associated with lipolysis, fatty acid/cholesterol absorption and transport, the Kennedy pathway, and retinol metabolism, consistent with increased hepatic fat accumulation. Moreover, several major histocompatibility complex (MHC) class II genes (*H2-Aa*, *H2-Ab1*, *H2-DMb1*, *Cd74*) were repressed, coincident with decreased macrophage and dendritic cell levels in the lamina propria, suggesting migration of antigen-presenting cells out of the intestine. In contrast, hepatic RNA-Seq analysis identified increased expression of MHC class II genes, as well as chemokines and chemokine receptors involved in macrophage recruitment (*Ccr1*, *Ccr5*, *Ccl5*, *Cx3cr1*), consistent with hepatic F4/80 labeling and macrophage infiltration into the liver. Collectively, these results suggest TCDD elicits changes that support hepatic lipid accumulation, macrophage migration, and the progression of hepatic steatosis to steatohepatitis.

Key words: jejunum; TCDD; toxicogenomics; macrophage; NAFLD; MetS

Metabolic syndrome (MetS), a constellation of disorders that includes obesity, insulin resistance, and dyslipidemia (Paschos and Paletas, 2009; Vanni *et al.*, 2010), is approaching pandemic levels (Ford *et al.*, 2010; Grundy, 2008). In the liver, MetS can manifest itself as nonalcoholic fatty liver disease (NAFLD), in which benign and reversible hepatic fat accumulation (steatosis) progresses to chronic steatohepatitis (steatosis with inflammation) and fibrosis (collagen deposition) (Alberti *et al.*, 2009; Olufadi and Byrne, 2008; Trauner *et al.*, 2010). Recent reports suggest the aryl hydrocarbon receptor (AhR) plays an underappreciated role in the development of MetS and NAFLD (Casals-Casas and Desvergne, 2011; Chen *et al.*, 2009;

Cimafranca *et al.*, 2004; Grun and Blumberg, 2009; Taylor *et al.*, 2013).

2,3,7,8-Tetrachlorodibenzo-*p*-dioxin (TCDD) is the prototypical ligand for a group of structurally diverse synthetic chemicals, natural products, and endogenous metabolites that activate the AhR (Denison *et al.*, 2011). Upon binding, the cytoplasmic AhR dissociates from AIP, p23 and Hsp90 chaperone proteins, translocates to the nucleus, and heterodimerizes with the AhR nuclear translocator (ARNT). The AhR/ARNT complex acts as a transcription factor, altering levels of gene expression primarily through binding to dioxin response elements (DREs) (Denison *et al.*, 2002; Hankinson, 1995); however, DRE-independent mechanisms of differential gene expression have also been reported (Beischlag *et al.*, 2008; Dere *et al.*, 2011b; Huang and Elferink, 2012).

In mice, a single bolus dose of TCDD induces hepatic steatosis and immune cell infiltration (Boverhof *et al.*, 2005; Kopec *et al.*, 2010b), with progression to steatohepatitis and fibrosis following repeated treatment (Pierre *et al.*, 2014). Our previous studies have shown that dietary fat rather than *de novo* synthesis is a primary source of lipids involved in TCDD-elicited hepatic steatosis. Dose-dependent hepatic increases in essential dietary fatty acids (ie, 18:2n6 and 18:3n3) were reported in TCDD-treated mice fed a high-fat diet but not a high-carbohydrate diet (Angrish *et al.*, 2012). Furthermore, TCDD increased hepatic levels of oleate (18:1) in *Scd1*-null mice incapable of desaturating stearate (18:0), while hepatic *de novo* fatty acid synthesis and beta oxidation gene expression were repressed (Angrish *et al.*, 2012; Forgacs *et al.*, 2012; Lee *et al.*, 2010). Based on these studies, we hypothesize that TCDD-mediated changes in intestinal function support the development of hepatic steatosis and its progression to steatohepatitis.

The intestine is divided into the duodenum, jejunum, ileum, and colon, with each segment differing in structure and absorptive function. Lipid absorption occurs predominantly in the jejunum, with compensatory uptake by the ileum as the fat load increases (Booth *et al.*, 1961). Dietary fats such as triglycerides (TAGs) are hydrolyzed in the lumen by lipases and the resulting free fatty acids are absorbed into intestinal epithelial cells (enterocytes) either by passive diffusion or active processes involving membrane transporters. Inside enterocytes, fatty acids are reassembled into TAGs and packaged with cholesterol and apolipoproteins into chylomicrons for transport to the liver via portal circulation (Hamilton, 1998). During digestion and nutrient absorption, the gastrointestinal tract is continuously exposed to foreign antigens and thus the intestine is equipped with organized lymphoid tissue such as Peyer's Patches, as well as individual innate immune cells including monocytes/macrophages, dendritic cells (DCs), and innate lymphoid cells scattered throughout the epithelium and lamina propria (Doe, 1989; Tomasello and Bedoui, 2013).

In this report, jejunal epithelial global gene expression and intestinal lamina propria immune cell populations were examined to further investigate intestine—liver interactions that may contribute to TCDD-elicited steatohepatitis in mice. Our results demonstrate that TCDD-elicited differentially expressed genes (DEGs) were associated with lipolysis, fatty acid/cholesterol absorption and transport, the Kennedy pathway, and retinol metabolism, consistent with increased hepatic fat accumulation. Furthermore, several major histocompatibility complex (MHC) class II genes involved in immune cell activation and antigen presentation exhibited reduced expression, coincident with decreased populations of macrophages, and DCs in the intestinal lamina propria. In contrast, hepatic macrophage levels increased in TCDD-treated animals, and thus we speculate that immune cells may be migrating from the intestine to the liver. Collectively, these results are consistent with jejunum—liver interactions that contribute to TCDD-elicited steatohepatitis.

MATERIALS AND METHODS

Animal Handling and Treatment

Female C57BL/6 mice weighing within 10% of each other were obtained from Charles River Laboratories (Portage, Michigan) on postnatal day 25 (PND25). Animals were housed in polycarbonate cages containing cellulose fiber chips (Aspen Chip Laboratory Bedding, Northeastern Products, Warrensberg, New York) in a 23°C environment with 30%–40% humidity and a 12-h light/dark cycle (7 AM to 7 PM). Mice were provided deionized water and Harlan Teklad 22/5 Rodent Diet 8940 (Madison, Wisconsin) *ad libitum*, and were acclimated for 4 days. Animals (N = 8) were orally gavaged with sesame oil vehicle (Sigma-Aldrich, St. Louis, Missouri), 0.001, 0.01, 0.03, 0.1, 0.3, 1, 3, 10, or 30 μg/kg TCDD (Dow Chemical Company, Midland, Michigan) every 4 days for a total of 28 days (7 exposures; Supplementary Figure S1A). For the high-dose female and male study, C57BL/6 mice (PND25) obtained from Charles River Laboratories (Kingston, New York) were housed in Innovive Innocages (San Diego, CA) with ALPHA-dri bedding (Shepherd Specialty Papers, Chicago, Illinois). Animals were fed *ad libitum* Harlan Teklad Rodent Diet 8940 and Aquavive water (Innovive). Beginning on PND28–31, animals (N = 8–16) were orally gavaged with either sesame oil vehicle (Sigma) or 30 μg/kg TCDD (Dow Chemical Company) every 4 days for a total of 28 days (7 exposures; Supplementary Figure S1B). All animal handling procedures were performed with the approval of the Michigan State University All-University Committee on Animal Use and Care.

Tissue Collection

On day 28, female mice from the dose-response study were weighed and blood was collected from the submandibular vein prior to cervical dislocation. Four intestinal sections were removed: duodenum (entire length up to the duodenojejunal flexure), jejunum (~6 cm section proximal to the duodenum), ileum (~6 cm section proximal to the caecum), and colon (entire length). Each section was flushed with Ca^{2+}/Mg^{2+}-free phosphate buffered saline (PBS; Sigma) and cut open longitudinally. An ~0.5 cm segment was removed from each of the 4 sections and fixed in 10% neutral buffered formalin (NBF; Sigma). Epithelium from the remaining sections were individually scraped into vials containing 1.3 ml TRIzol (Invitrogen, Carlsbad, California), frozen in liquid nitrogen, and stored at −80°C. Liver, pancreas, and gonadal white adipose tissue (gWAT) were removed, weighed, frozen in liquid nitrogen, and stored at −80°C. The right lobe of the liver was sectioned and either fixed in 10% NBF (Sigma) for histological analyses or frozen in Tissue-Tek O.C.T. compound (Sakura, Torrance, California) for Oil Red O (ORO) staining of neutral lipids.

Flow Cytometry

On day 28, female and male mice from the high-dose study were sacrificed by cervical dislocation and intestinal lamina propria cells were collected for flow cytometry analysis using a modified protocol (Geem *et al.*, 2012). Briefly, the small intestine was removed and cut into the proximal intestine consisting of the duodenum and jejunum, and the distal intestine consisting of the ileum. Each section was flushed with Ca^{2+}/Mg^{2+}-free PBS, opened longitudinally, and cut into ~1.5 cm pieces. The proximal and distal intestinal pieces were placed in separate conical tubes

containing 10 ml of pre-warmed (37°C) Ca^{2+}/Mg^{2+}-free Hank's Balanced Salt Solution (HBSS; Sigma) with 5% heat-inactivated fetal bovine serum (HBSS/FBS) and 2 mM EDTA. Enterocytes were dissociated using two 20-min rounds of horizontal shaking (~250 revolutions per minute [rpm]) at 37°C, transferring the tissue to fresh HBSS/FBS with 2 mM EDTA after the first 20 min. The contents of each tube were strained, intestinal pieces minced, and tissue transferred to a conical tube containing 10 ml of pre-warmed HBSS/FBS with 1.5 mg/ml Collagenase Type IV from *Clostridium histolyticum* (Sigma) and 40 μg/ml Deoxyribonuclease I from bovine pancreas (Sigma). To digest the tissue, the proximal and distal samples were horizontally shaken (~250 rpm) at 37°C for 10 and 15 min, respectively, followed by 10 s of vortexing. Each tube was then filtered through a 70 μm cell strainer (Falcon, Tewksbury, Massachusetts) into a conical tube containing HBSS/FBS. The strained cells were pelleted at 1500 rpm for 5 min, washed twice in ice-cold HBSS/FBS and resuspended in ice-cold FACS buffer (Ca^{2+}/Mg^{2+}-free HBSS with 1% bovine serum albumin (Sigma) and 0.1% sodium azide (Sigma), pH 7.6).

Proximal and distal intestinal suspensions were quantified using the TC20 Automated Cell Counter (Bio-Rad, Hercules, California) with ≥ 90% viability confirmed by visual assessment of Trypan Blue (Life Technologies, Grand Island, New York) staining. Cells (10^6) were pelleted and surface Fc receptors blocked with anti-mouse CD16/CD32 antibody (2.4G2; BD Biosciences, San Jose, California) for 10 min on ice. Cells were then labeled for 20 min on ice with an antibody cocktail. The immune cell panel cocktail consisted of fluorescently-labeled CD3e (145-2C11; BioLegend, San Diego, California), CD4 (GK1.5; BioLegend), CD8a (53-6.7; BioLegend), CD19 (6D5; BioLegend), F4/80 (BM8; eBioscience, San Diego, California), and NK1.1 (PK136; BioLegend) anti-mouse antibodies. The DC cocktail consisted of fluorescently-labeled CD11b (M1/70), CD11c (N418), and CD103 (2E7) BioLegend anti-mouse antibodies. Following labeling, cells were washed with ice-cold FACS buffer, re-pelleted, fixed with Cytofix (BD Biosciences) for 15 min on ice, and resuspended in ice-cold FACS buffer for subsequent analysis. Compensation and voltage settings of fluorescent parameters were performed using single color labeling controls. Fluorescent labeling of the cell suspensions was analyzed using a BD FACSCanto II flow cytometer (BD Biosciences).

TCDD Tissue Levels

Hepatic TCDD levels were quantified as previously described (Kopec *et al.*, 2011). Briefly, tissues were weighed, spiked with $^{13}C_{12}$-2,3,7,8-TCDD, digested with hydrochloric acid, and subjected to extraction and clean-up procedures. Prior to injection, $^{13}C_{12}$-1,2,3,4-TCDD was added to the concentrated extracts. Calibration standards containing 2,3,7,8-TCDD, $^{13}C_{12}$-2,3,7,8-TCDD and $^{13}C_{12}$-1,2,3,4-TCDD were first analyzed by high-resolution gas chromatography/high-resolution mass spectrometry (HRGC/HRMS), followed by solvent blanks and then the extracts. The HRGC/HRMS system was a Hewlett Packard 6890N HRGC interfaced to a Waters Autospec Ultima HRMS. Chromatographic separations were carried out in constant flow mode (Helium, 1 ml/min) on a 60 m DB5 (0.25 mm ID, 0.25 μm film thickness) column. The HRMS was operated in EI+ selective ion recording mode at a mass resolving power of 10 000 or greater.

Clinical Chemistry

Total serum cholesterol, TAGs, and glucose were determined using commercially available kits (Pointe Scientific, Canton, Michigan) according to manufacturer's protocol. All assays were performed using an Infinite M200 plate reader (Tecan, Durham, North Carolina).

Histological Analysis

All tissue processing for histology was performed by the Michigan State University Investigative HistoPathology Laboratory (https://humanpathology.natsci.msu.edu, last accessed September 24, 2015). Formalin-fixed intestinal and hepatic tissues were processed and vacuum infiltrated with paraffin using a Tissue-Tek VIP 2000 tissue processor (Sakura) followed by embedding with the Thermo Fisher HistoCentre III embedding station (Thermo Fisher, Waltham, Massachusetts). Paraffin blocks were sectioned at 4–5 μm with a Reichert Jung 2030 rotary microtome (Reichert, Depew, New York) and dried for 2–24 h at 56°C to ensure adherence to the slides. For lipid staining, liver sections frozen in O.C.T. compound were sectioned at 6 μm, fixed in 10% NBF for 5 min, rinsed with water, and immersed in 100% propylene glycol for 5 min.

Intestinal sections from vehicle and 30 μg/kg TCDD-treated female mice (N = 3) were stained with hematoxylin and eosin (H&E), and macrophages in the intestinal wall were labeled using a monoclonal anti-mouse F4/80 antibody (1:100 dilution; AbD Serotec, Raleigh, North Carolina). Liver sections from female mice were stained with H&E for general assessment of histological features and identification of doses requiring further assessment using alternate staining or immunohistochemical analyses. Lipid staining was performed by ORO as previously described (Kopec *et al.*, 2010b). Macrophage infiltration was determined for vehicle, 3, 10, and 30 μg/kg TCDD-treated mice using the monoclonal anti-mouse F4/80 antibody as described above. Further characterization of the inflammatory response was achieved by labeling for eosinophils (vehicle, 3, 10, and 30 μg/kg TCDD) using a rat anti-mouse major basic protein (MBP) antibody (1:500; Mayo Clinic, Scottsdale, Arizona) and the presence of alternatively activated macrophages (vehicle, 3, 10, and 30 μg/kg TCDD) was assessed using a goat polyclonal anti-mouse Chitinase 3-like 3/ECF-L antibody (Ym1; 1:1500 dilution; R&D Systems, Minneapolis, Minnesota).

Quantitation of histological features was performed using the Quantitative Histological Analysis Tool (QuHAnT) (Nault *et al.*, 2015a). Briefly, slides were digitized at 20× magnification using an Olympus Virtual Slide System VS110 (Olympus, Pennsylvania). Digitized slides were then sampled at 100% coverage using the Visiomorph Microimager (Visiopharm, Denmark). Each image was visually inspected for quality, and flawed images (eg, debris, bubbles, false positives) were removed prior to analysis. Hue, Saturation, and Value image segmentation values for feature extraction and background extraction were determined using ImageJ (http://imagej.nih.gov/ij/, last accessed September 24, 2015) and are provided in Supplementary Table S1. Volume densities were estimated as the sum of positive hits ($P_{positive}$ staining) divided by the total number of tissue hits (P_{tissue}) for each section ($V_v = (P_{positive\ staining}/P_{tissue}) \times 100$). Assessment of micro- and macrovesicular steatosis using ORO stained liver sections was determined using a cutoff of 176 μm^2 estimated based on a diameter of 15 μm previously reported to identify macro lipid vacuolization (Zaitoun *et al.*, 2001).

RNA Isolation

Frozen intestinal epithelium scrapings stored in TRIzol were homogenized using a Mixer Mill 300 tissue homogenizer (Retsch, Germany). Total RNA was isolated according to the manufacturer's protocol with an additional acid phenol:chloroform (Sigma) extraction, and resuspended in RNase-free RNA storage solution (Ambion Inc., Austin, Texas). RNA was quantified using a Nano-drop spectrophotometer (Thermo Scientific, Wilmington, Delaware) at 260 nm and purity was assessed by

calculating the A_{260}/A_{280} ratio. Quality of the RNA was visually evaluated by electrophoresis of 2 μg on a 1% denaturing formaldehyde-agarose gel.

Microarray Analysis

Dose-dependent gene expression changes were examined using mouse 4 × 44K Agilent whole-genome oligonucleotide microarrays (version 1, Agilent Technologies, Inc., Santa Clara, California). Hepatic RNA from treated and control samples were cohybridized to individual arrays according to the manufacturer's protocol (Agilent Manual: G4140-90040 v. 5.7). All hybridizations were performed with 3 independent biological replicates (ie, RNA samples were not pooled) and 2 independent labelings (Cy3 and Cy5 dye swaps). Microarrays were scanned at 532 nm (Cy3) and 635 nm (Cy5) on a GenePix 4000B scanner (Molecular Devices, Union City, California). Images were analyzed for feature and background intensities using GenePix Pro 6.0 software (Molecular Devices). All data passed our laboratory quality assurance protocol (Burgoon *et al.*, 2005) and were managed in TIMS dbZach data management system (Burgoon and Zacharewski, 2008). The complete microarray data set has been deposited in Gene Expression Omnibus (GEO; accession number GSE70379) database and is available as Supplementary Table S2.

Data were normalized using a semiparametric approach (Eckel *et al.*, 2005) in SAS v9.3 (SAS Institute Inc., Cary, North Carolina). Posterior probability P1(*t*) values were calculated using an empirical Bayes method based on a per gene and dose basis using model-based *t*-values (Eckel *et al.*, 2004). For TCDD-mediated differential gene expression, fold changes were calculated relative to vehicle controls. Genes were considered to be differentially expressed if |fold change| ≥ 1.5 and statistical P1(*t*) value ≥ 0.999 at 1 or more doses.

Dose-Response Modeling

Dose-response modeling was performed using the ToxResponse Modeler (Burgoon and Zacharewski, 2008). Median effective dose (ED_{50}) values for features exhibiting a sigmoidal response were reported if within the experimental dose range (0.01–30 μg/kg). Estimation of benchmark dose (BMD) and BMD lower confidence limit (BMDL) was performed using BMDExpress (Yang *et al.*, 2007). A benchmark response factor of 1.349 was chosen to represent a 10% change in transcript levels compared with vehicle controls. Normalized linear microarray signal intensities for each feature were fit to Hill, linear (1° polynomial), 2° polynomial, or power dose-response models and the best globally fitting model with the least complexity was selected following the criteria previously published by U.S. EPA (Bhat *et al.*, 2013).

Functional Annotation

DEGs were analyzed for enriched functions using the database for annotation, visualization, and integrated discovery (DAVID) v6.7. Only gene ontology (GO) biological processes were considered for the enrichment analysis. Functional groups with an enrichment score (ES) ≥ 1.3 were considered significantly enriched, representing the −log scale geometric mean *P* value of .05.

Computational Putative DRE Identification

Putative DREs (pDREs) were previously identified (Dere *et al.*, 2011a). Briefly, gene regulatory regions (10 kb upstream of the transcription start site together with 5′- and 3′-untranslated regions) and coding sequence obtained from the University of California, Santa Cruz (UCSC) Genome Browser for mouse (mm9, build 37) were computationally searched for the DRE core consensus sequence 5′-GCGTG-3′. Each identified core was extended by 7 bp upstream and downstream, and the resulting 19 bp sequences were scored using a position weight matrix constructed from *bona fide* functional DREs. Matrix similarity scores ≥ 0.8473 were considered to be pDREs.

Statistical Analysis

All statistical analyses were performed in SAS 9.3 (SAS Institute Inc.). Unless otherwise stated, differences between groups were considered significant when $P \leq .05$.

RESULTS

Gross Pathology and Clinical Chemistry

We have previously established that a single bolus dose of 30 μg/kg TCDD elicits hepatic fat accumulation that is almost completely reversed after 4 weeks following cessation of treatment (Kopec *et al.*, 2013), consistent with a half-life of 8.5–12 days in mice (Birnbaum, 1986; Gasiewicz *et al.*, 1983; Kopec *et al.*, 2013) compared with 1.3–11.3 years in humans (Michalek *et al.*, 1996; Pirkle *et al.*, 1989; Sorg *et al.*, 2009; Wolfe *et al.*, 1994). In order to approach steady-state TCDD levels, mice were gavaged every 4 days for 28 days to investigate the longer-term effects of TCDD exposure. Hepatic TCDD levels exhibited a dose-dependent increase (Table 1) that exceeded levels of a single bolus dose by ~4-fold (Boverhof *et al.*, 2005). In comparison, hepatic TCDD levels range from 0.2 to 5.4 ppt in humans (Leung *et al.*, 1990), ~10-fold less than the levels achieved with 0.001 μg/kg.

In this study, TCDD did not affect terminal body weight, with the exception of a negligible increase at 0.03 μg/kg (Table 1). However, relative liver weight (RLW) displayed a 21%–30% dose-dependent increase at 3, 10, and 30 μg/kg TCDD, whereas the relative gWAT weight (RgWATW) decreased by 49% at 30 μg/kg TCDD (Table 1). No change in terminal pancreas weight was observed (results not shown).

Serum cholesterol levels decreased from 121.5 to 88.3 mg/dl at 30 μg/kg TCDD, consistent with trends reported following a single bolus dose of 30 μg/kg TCDD (Angrish *et al.*, 2013; Boverhof *et al.*, 2005). Although TAG levels exhibited a decrease, it did not achieve statistical significance. In contrast, serum TAG levels were elevated in fed mice following a single bolus dose of 30 μg/kg TCDD, but unchanged in fasted mice receiving the same dose, suggesting duration of exposure and access to chow affect the lipidemic profile (Angrish *et al.*, 2013; Boverhof *et al.*, 2005). Glucose levels were unchanged in both the current study (Table 1) and in mice following a single bolus dose (Boverhof *et al.*, 2005).

Jejunal Differential Gene Expression

The jejunum is the segment of the small intestine predominantly responsible for dietary fat absorption. Dose-dependent differential gene expression in the jejunal epithelium of female mice was evaluated using Agilent 4X44K whole-genome oligonucleotide microarrays containing 41 267 probes representing ~21 308 unique genes. Empirical Bayesian analysis identified 439 DEGs (|fold change| ≥ 1.5, P1(*t*) ≥ 0.999) across 1 or more doses (Figure 1A). The number of unique DEGs at each dose reveals a bimodal distribution with the largest number differentially expressed at 30 μg/kg TCDD and a smaller peak at 0.3 μg/kg TCDD (Figure 1B). Similar anomalies have been observed in previous studies within the mid-dose range (Kopec *et al.*, 2010a). Salivary amylase 1 (*Amy1*) and pancreatic carboxypeptidase A2 (*Cpa2*) were among the most induced genes at 27.7- and 24.2-fold, respectively, whereas immunoglobulin joining chain (*Igj*) and cubilin (*Cubn*) were the most repressed at 3.9- and 3.1-fold,

TABLE 1. Gross Pathology, Serum Clinical Chemistry, and Hepatic TCDD Levels

Dose (μg/kg)	Gross Pathology			Serum Clinical Chemistry			Hepatic TCDD Levels	
	Body Weight (g)	RLW (%)	RgWATW (%)	Cholesterol (mg/dl)	Glucose (mg/dl)	TAG (mg/dl)	Repeated (ppt)	Acute[a] (ppt)
0	17.1 ± 1.1	4.83 ± 0.12	1.36 ± 0.12	121.5 ± 3.0	103.2 ± 3.4	112.8 ± 8.2	61 ± 59	72 ± 98
0.001	17.5 ± 0.7	4.74 ± 0.26	1.13 ± 0.12	118.0 ± 4.4	107.1 ± 3.5	106.0 ± 8.4	48 ± 31	14 ± 9
0.01	17.7 ± 1.0	4.42 ± 0.58	0.97 ± 0.12	117.7 ± 4.6	104.1 ± 2.8	95.6 ± 6.1	122 ± 38	35 ± 12
0.03	18.2 ± 1.6*	5.07 ± 0.20	0.98 ± 0.11	119.2 ± 2.7	108.4 ± 4.3	101.8 ± 8.3	297 ± 95*	NM
0.1	17.1 ± 0.7	5.10 ± 0.17	1.06 ± 0.07	116.8 ± 2.5	107.4 ± 2.7	94.1 ± 6.9	1553 ± 368*	418 ± 84
0.3	18.1 ± 1.2	5.54 ± 0.17	1.10 ± 0.09	119.4 ± 1.5	105.4 ± 2.1	102.0 ± 4.3	5600 ± 1383*	NM
1	17.9 ± 1.5	5.57 ± 0.19	1.22 ± 0.11	114.2 ± 3.2	100.8 ± 3.4	100.4 ± 9.0	19 533 ± 5008*	5278 ± 2087
3	17.6 ± 1.2	5.86 ± 0.22*	1.13 ± 0.09	110.4 ± 2.5	102.6 ± 3.5	103.6 ± 9.7	57 200 ± 10 047*	NM
10	17.6 ± 1.3	6.26 ± 0.22*	0.93 ± 0.17	95.8 ± 4.3	110.2 ± 4.6	98.3 ± 11.3	165 333 ± 34 818*	61 750 ± 10 546
30	17.0 ± 1.0	6.22 ± 0.18*	0.69 ± 0.10*	88.3 ± 2.2*	102.2 ± 4.0	91.6 ± 6.4	653 666 ± 109 038*	NM

NM indicates not measured.
[a]Single bolus dose after 24 h (Boverhof *et al.*, 2005).
*Indicates $P \leq .05$ compared with vehicle control.

respectively. Several AhR battery genes including *Cyp1a1*, *Cyp1a2,* and TCDD-inducible poly(ADP-ribose) polymerase (*Tiparp*) were also induced 4.7-, 3.9- and 2.7-fold, respectively, at 30 μg/kg TCDD.

Dose-Response Modeling

ToxResponse Modeler (Burgoon and Zacharewski, 2008) identified 264 sigmoidal, 28 Gaussian, and 47 exponential responses, with 123 features not fitting an appropriate model (Figure 2A). ED_{50} values for sigmoidal dose-responsive features ranged between 0.019 and 29.0 μg/kg TCDD. The frequency distribution for these ED_{50} values followed a step-wise pattern with peaks at 0.4, 1.1, and 3.2 μg/kg TCDD (Figure 2B).

BMDExpress (Yang *et al.*, 2007) was also used to analyze the dose-response behavior of 368 unique DEGs, following removal of 71 genes containing a blank intensity value at 1 or more doses. Using EPA criteria (Bhat *et al.*, 2013), 10 hill, 53 linear, 24 second degree (2°) polynomial, and 37 power responses were identified. The remaining 291 features failed to meet modeling criteria defined by EPA (Figure 2A). The frequency distribution of BMDL values for all hill, linear, 2° polynomial, or power responses also exhibited peaks at 0.4, 1.1, and 3.2 μg/kg TCDD, consistent with the step-wise ED_{50} distribution pattern (Figure 2B).

Functional Enrichment Analysis

DAVID identified 11 significantly enriched functional clusters (ES ≥ 1.3), including 3 lipid-related processes: (1) lipid transport and metabolism (ES = 3.04), (2) lipoprotein receptor activity and binding (ES = 1.62), and (3) lipid homeostasis (ES = 1.60) (Figure 3A). A total of 38 lipid-related DEGs were identified using representative GO terms (lipid metabolic process GO:0006629; lipid binding GO:0008289; lipid transport GO:0006869), with manually curated additions (Figure 3B). pDREs were identified in 30 of 38 lipid-related DEGs, suggesting involvement of DRE-dependent and -independent mechanisms. Several lipases were upregulated, including pancreatic lipase (*Pnlip*), primarily responsible for hydrolysis of dietary TAGs into free fatty acids, and its essential cofactor pancreatic colipase (*Clps*), induced 16.4 - and 2.5-fold, respectively. Monoglyceride lipase (*Mgll*), alkaline ceramidase 1 (*Acer1*), and lipoprotein lipase (*Lpl*) were also upregulated 1.5- to 1.8-fold, suggesting TCDD enhances dietary fat hydrolysis. Various lipid transporters were also differentially expressed such as long-chain fatty acid transporter Cd36 antigen (*Cd36*; 1.7-fold), whereas cholesterol transporters, including NPC1-like 1 (*Npc1l1*) and ATP-binding cassette A1 (*Abca1*), were repressed 1.6- and 2.0-fold, respectively, and intracellular cholesterol binding protein StAR-related lipid transfer domain containing 4 (*Stard4*) was repressed 1.5-fold. This would suggest that absorption of dietary cholesterol is reduced by TCDD, consistent with lower serum cholesterol levels.

In addition, several genes involved in the metabolism of glycerophospholipids, specifically phosphatidylcholine (PC), were differentially expressed. Prior to absorption, dietary PC undergoes phospholipase A2 (PLA2)-mediated hydrolysis to yield free fatty acids and lysoPC, which are then taken up by enterocytes (Cohn *et al.*, 2010). Phospholipase B domain containing 1 (*Plbd1*), which contains PLA2 activity, was repressed 1.7-fold, suggesting PC absorption may be impaired. Choline kinase α (*Chka*), phosphate cytidylyltransferase 1 choline α (*Pcyt1a*), and choline phosphotransferase 1 (*Chpt1*) were repressed 1.5-, 1.6-, and 1.8-fold, respectively. Interestingly, these enzymes catalyze the 3 consecutive steps of the PC branch of the Kennedy pathway, suggesting *de novo* synthesis of PC from choline and diacylglycerol (DAG) is repressed by TCDD. DAG kinase η (*Dgkh*), which catalyzes the phosphorylation of DAG to DAG-3-phosphate, was induced 3.7-fold which could deplete DAG levels, further limiting the Kennedy pathway. Additionally, glycerophosphocholine phosphodiesterase GDE1 homolog (*Gpcpd1*), responsible for the cleavage of choline from glycerol-3-phosphocholine, was induced 2.1-fold. This, with Kennedy pathway repression, could increase free choline in jejunal enterocytes.

Retinol (vitamin A) metabolism genes were also differentially expressed following TCDD treatment. For example, β-carotene 15,15′-monooxygenase (*Bcmo1*), responsible for converting β-carotene to retinal, was induced 6.7-fold. Interestingly, lipid transporters responsible for β-carotene uptake, including *Cd36* and scavenger receptor class B1 (*Scarb1*) (Reboul, 2013), were also induced by TCDD. In contrast, retinol dehydrogenase 16 (*Rdh16*), which catalyzes the reduction of retinal to retinol, was repressed 1.6-fold, while *Rdh7* was repressed 1.7-fold. Moreover, cellular retinol binding protein 7 (*Rbp7*) and plasma retinol binding protein 4 (*Rbp4*), were induced 2.2- and 1.5-fold, respectively.

An immune cell activation and antigen presentation cluster was also enriched (ES = 1.62) (Figure 3A). A total of 37 immune-related DEGs were identified using a representative GO term (immune system process GO:0002376) followed by manual

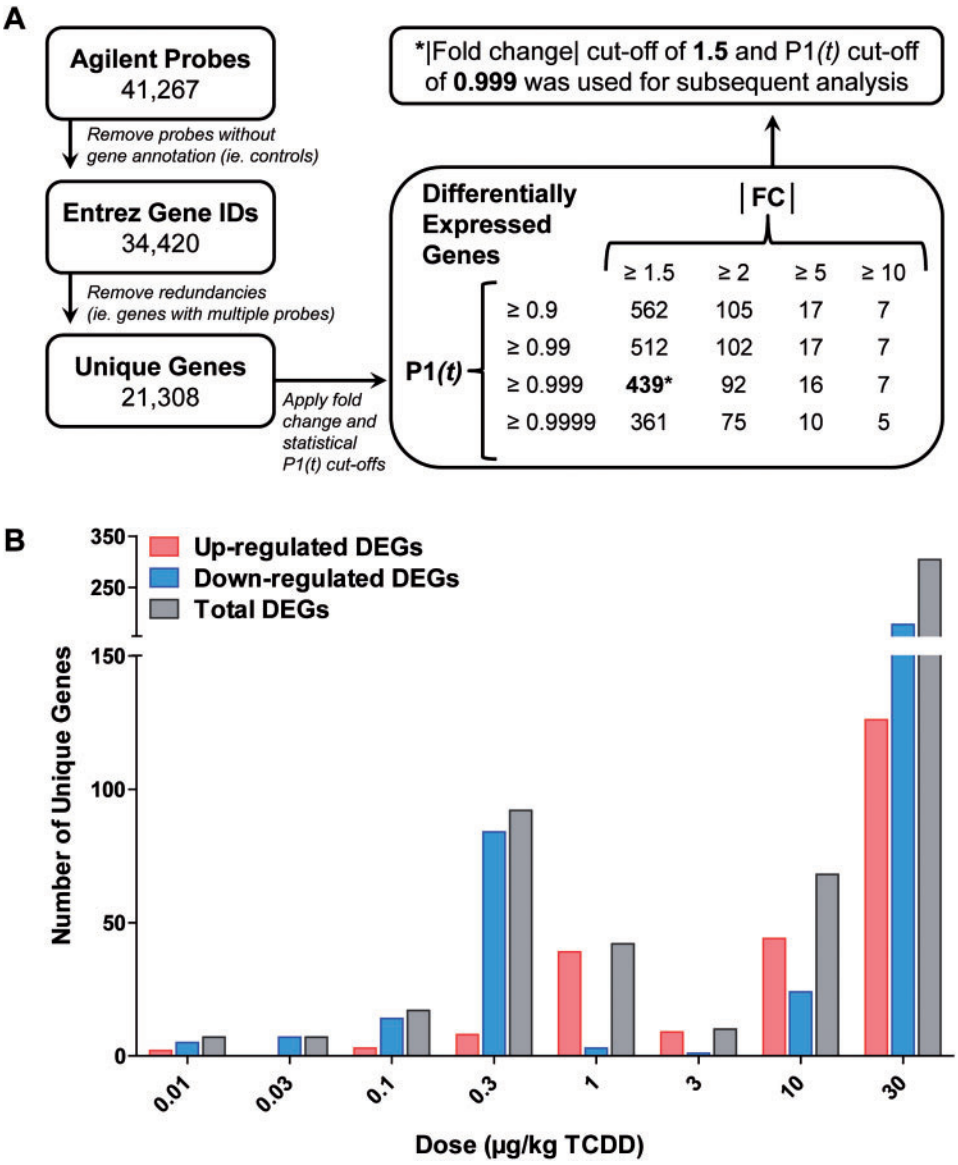

FIG. 1. Microarray analysis of dose-dependent jejunal epithelial differential gene expression in female C57BL/6 mice treated by oral gavage with sesame oil vehicle or 0.01–30 µg/kg TCDD every 4 days for 28 days. A, Agilent 4X44K whole-genome microarray data were filtered using |fold change| ≥ 1.5 and P1(t) ≥ 0.999 criteria, identifying 439 genes differentially expressed at 1 or more doses. B, The number of upregulated, downregulated, and total differentially expressed unique genes at each dose.

curation, of which 30 were down-regulated (Figure 3C). This includes several MHC class II genes (*H2-Aa*, *H2-Ab1*, *H2-DMb1*, *Cd74*) which were repressed 1.6- to 1.8-fold. Additionally, several genes expressed predominantly by immune cells (*Cd52*, *Lair1*), macrophages (*Irgm1*, *Pirb*, *Ifi44*), T cells (*Thy1*), and B cells (*Tnfrsf13b*, *Tnfrsf17*) were repressed. The absence of DREs in 28 of 37 immune-related genes suggests that DRE-independent mechanisms are involved in TCDD-elicited intestinal immune cell effects.

Intestinal Immune Cell Population Changes

Previous studies have reported TCDD-elicited differential expression of genes associated with immune cell activation and antigen presentation in the mouse liver (Boverhof *et al.*, 2005; Kopec *et al.*, 2013). As reported with the jejunal responses in this study, TCDD-elicited hepatic immune DEGs were predominantly independent of pDREs. Further investigation determined that the hepatic immune response was due to the dose-dependent infiltration of immune cells rather than DRE-dependent changes in gene expression (Boverhof *et al.*, 2005). Therefore, histopathology and flow cytometry were used to examine the possibility that decreased expression of immune-related genes was attributed to changes in intestinal immune cell populations.

No histological lesions were noted in the duodenum, jejunum, ileum, and colon of TCDD-treated mice. Moreover, visual assessment and quantitative analysis of F4/80 positive labeling using QuHAnT, an in-house developed, computational high throughput tool (Nault *et al.*, 2015a), detected no changes in macrophage populations (data not shown), although substantial interanimal variability in the number of F4/80-positively labeled cells was observed.

The intestinal immune system includes effector lymphocytes interspersed in the epithelial lining, with the majority of

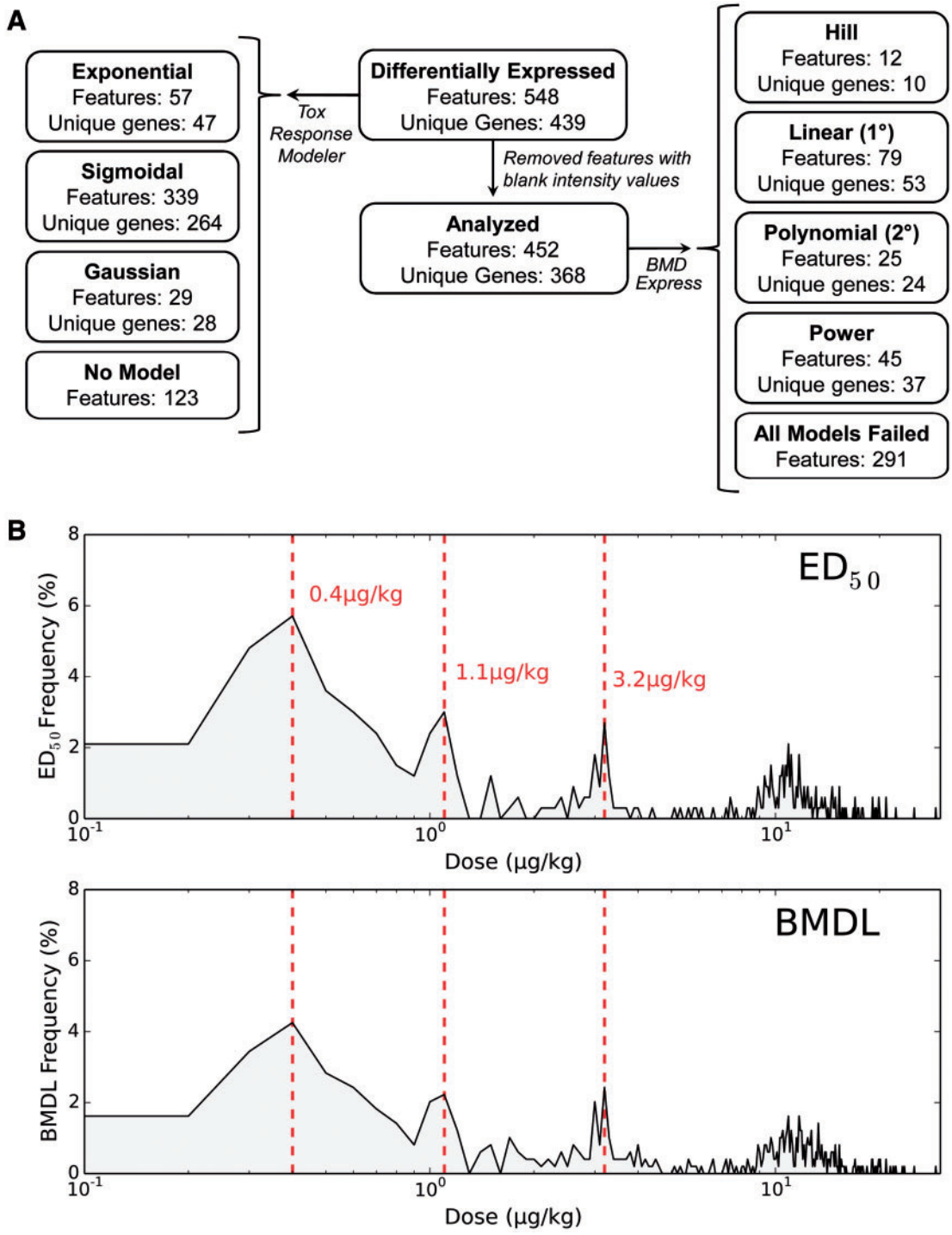

FIG. 2. Dose-response modeling of jejunal epithelial differentially expressed genes (DEGs) in female C57BL/6 mice treated by oral gavage with sesame oil vehicle or 0.01–30 µg/kg TCDD every 4 days for 28 days. A, Summary of ToxResponse Modeler (left) and BMDExpress (right) dose-response modeling for jejunal epithelial DEGs. B, Frequency distribution of ED_{50} values for 339 sigmoidal features (top) and bench mark dose lower confidence limit (BMDL) (bottom) values for 161 features exhibiting hill, linear, 2° polynomial, or power responses. The distributions reveal peaks at 0.4, 1.1, and 3.2 µg/kg TCDD, suggesting a dose-dependent step-wise response in differential gene expression.

scattered immune cells and lymphoid aggregates including Peyer's Patches located immediately below the epithelium in the lamina propria (Tomasello and Bedoui, 2013). In order to focus on immune cell populations within the lamina propria, the epithelial layer was removed prior to labeling with a cocktail consisting of anti-mouse CD3, CD4, CD8, CD19, F4/80, and NK1.1 antibodies to investigate total T cell, T helper cell, cytotoxic T cell, B cell, mature macrophage, and natural killer cell populations, respectively (Figure 4A). F4/80$^+$ macrophages decreased 32% and 30% in the proximal and distal intestine, respectively, of female mice, and 29% in the proximal intestine of male mice, suggesting macrophage reductions in the lamina propria. There

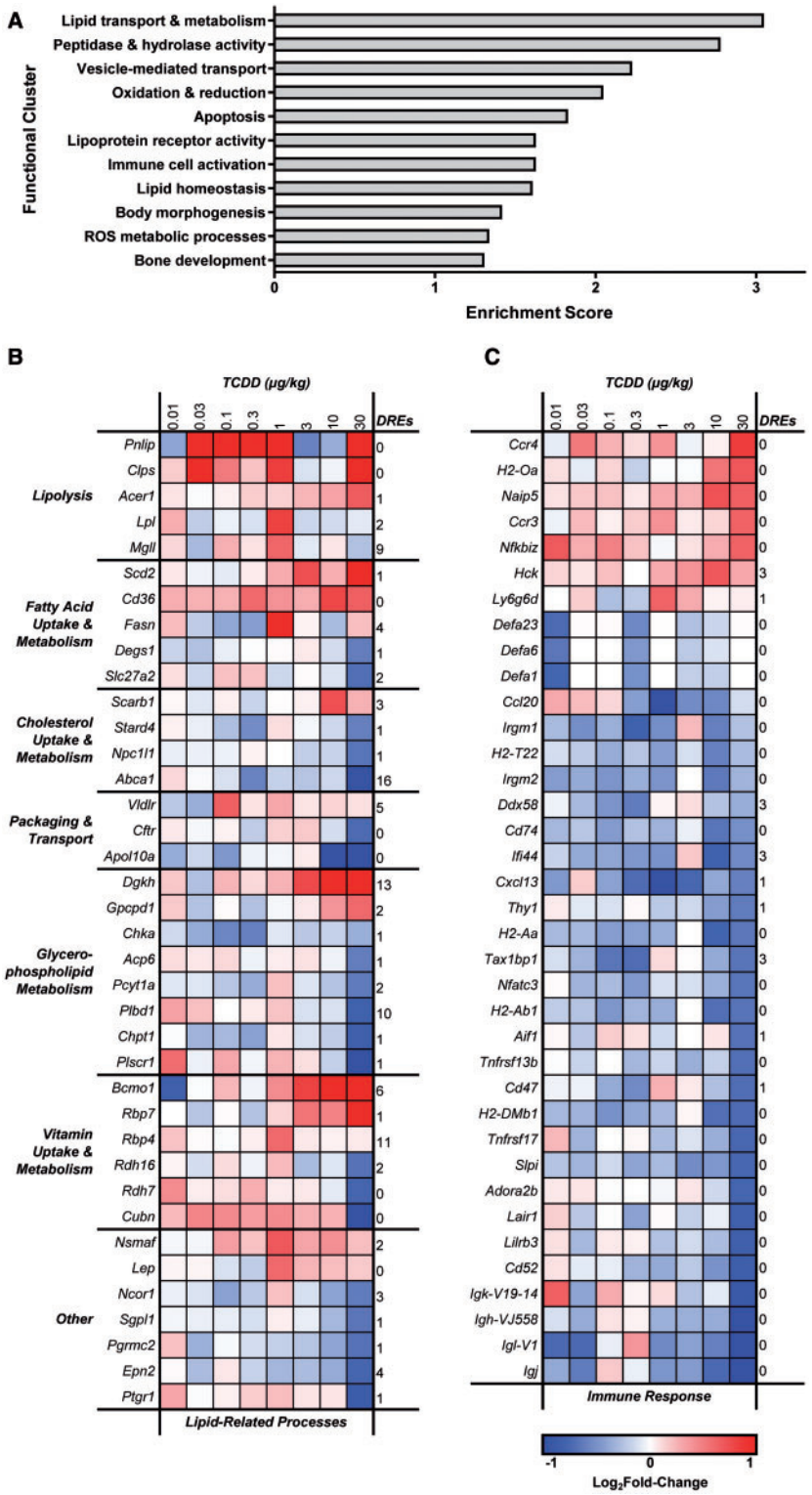

FIG. 3. Functional analysis of jejunal epithelial differentially expressed genes (DEGs) in female C57BL/6 mice treated by oral gavage with sesame oil vehicle or 0.01–30 μg/kg TCDD every 4 days for 28 days. A, Functional clusters identified using the Database for Annotation, Visualization and Integrated Discovery (DAVID). Scores ≥ 1.3 are considered significantly enriched. B, Heat map of DEGs associated with lipid-related processes. C, Heat map of DEGs associated with immune system processes. The number of pDREs (MS ≥ 0.8473) is indicated in the last column on the right of each heat map.

was also a 65% decrease in NK1.1$^+$ natural killer cells in male mice and a 68% decrease in CD4$^+$ lymphocytes in female mice in the proximal intestine, with a 28% decrease in CD3$^+$ T cells in male mice, and a 45% decrease in CD19$^+$ B cells in female mice in the distal intestine. These results are consistent with TCDD-elicited depletion of several populations of immune cells in the lamina propria, including natural killer cells, T helper cells, total T cells, and B cells.

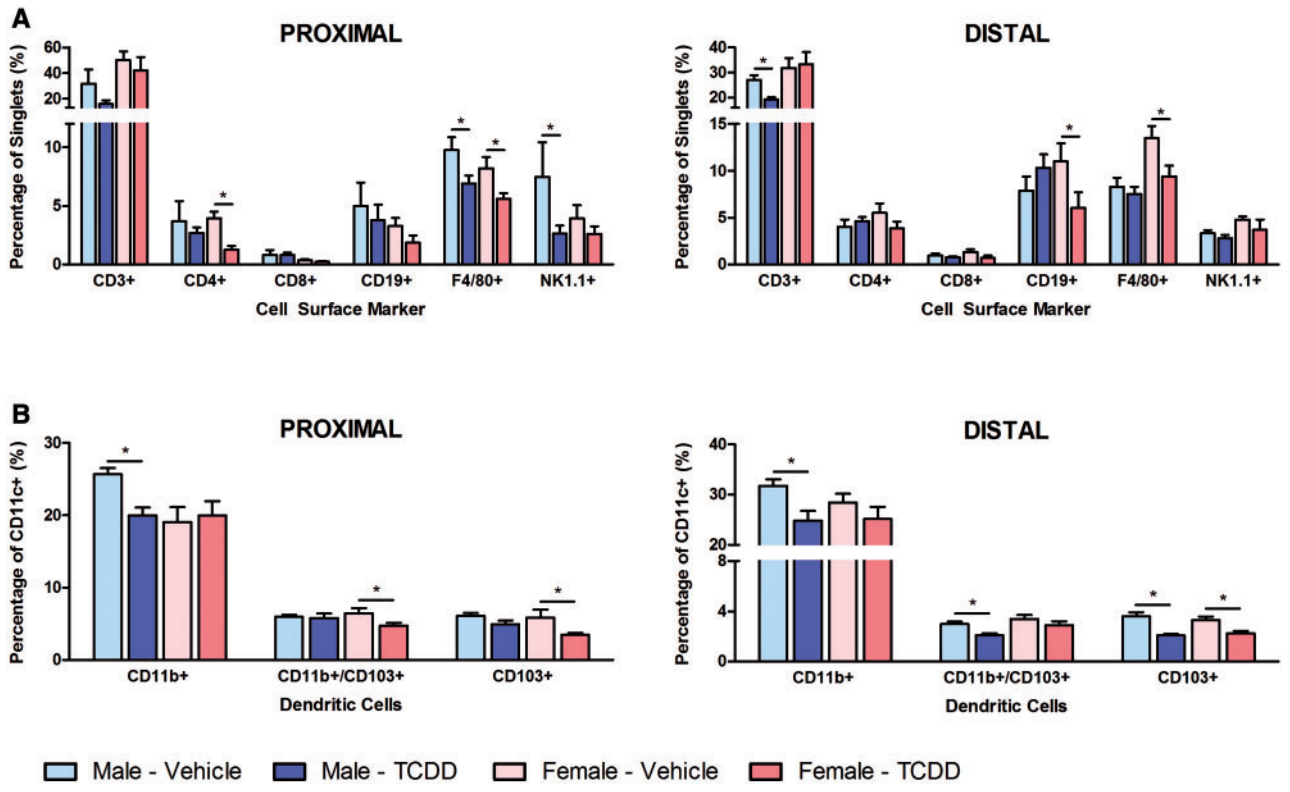

FIG. 4. Flow cytometry analysis of TCDD-mediated effects on immune cell populations within the intestinal lamina propria. Female and male mice were treated by oral gavage with either sesame oil vehicle or 30 μg/kg TCDD every 4 days for 28 days. Single cell suspensions prepared from the lamina propria were labeled with either (A) immune cell panel or (B) dendritic cell subpopulation antibodies. Immune cell panel results are expressed as the average percentage of singlets expressing various cell surface receptors ± standard error of the mean (SEM; $N \geq 3$), while dendritic cell subpopulations are expressed as the average percentage of $CD11c^+$ cells co-expressing CD11b and/or CD103 ± SEM ($N \geq 12$). Asterisks (*) indicate a significant difference ($P \leq .05$) compared with vehicle control determined by standard *t*-test performed using SAS 9.3.

A second antibody cocktail consisting of anti-mouse CD11b, CD11c, and CD103 antibodies examined 3 DC subpopulations including (1) $CD11c^+$ $CD11b^+$ $CD103^-$ DCs (herein referred to as $CD11b^+$ DCs), (2) $CD11c^+$ $CD11b^-$ $CD103^+$ DCs (herein referred to as $CD103^+$ DCs), and (3) $CD11c^+$ $CD11b^+$ $CD103^+$ DCs (herein referred to as double positive DCs) (Figure 4B). Within the $CD11c^+$ population, $CD11b^+$ DCs decreased 22% in both the proximal and distal intestine of male mice. Furthermore, $CD103^+$ DCs decreased 41% and 32% in the proximal and distal intestine, respectively, of female mice, and decreased 43% in the distal intestine of male mice. In addition, double positive DCs decreased 26% in the proximal intestine of female mice, and 30% in the distal intestine of male mice. Therefore, TCDD-elicited intestinal immune cell population changes appear to exhibit some sex and intestinal region specificity. Collectively, TCDD reduced several immune cell populations consistent with the decrease in jejunal immune-related gene expression.

Twenty-eight Day TCDD-Mediated Liver Effects

In order to examine jejunum–liver interactions, differential gene expression in the jejunal epithelium was compared with hepatic RNA-Seq data (GEO accession number GSE62903) from the same study (Nault *et al.*, 2015b) (Figure 5A). Empirical Bayes analysis identified 1172 hepatic DEGs ($|\text{fold change}| \geq 2.0$, $P1(t) \geq 0.8$) across 1 or more doses. Comparison with the 439 jejunal DEGs from the current study identified 53 DEGs common to both the jejunum and the liver, whereas 386 and 1119 DEGs were unique to the jejunum and liver, respectively (Supplementary Table S3). DAVID analysis of the common DEGs identified 2 enriched clusters functionally associated with antigen processing and presentation via MHC class II (ES = 3.99) and oxidative and reductive processes (ES = 2.75). Manual curation also revealed that several common DEGs were associated with lipid metabolism. Expression of common DEGs associated with these functions was compared across the 2 tissues (Figure 5B), revealing both consistent and divergent regulation. As expected, classical AhR battery genes *Cyp1a1* and *Cyp1a2* were induced in both tissues. Most lipid metabolism DEGs were also induced in both tissues. In contrast, fatty acid synthase (*Fasn*) and *Gpcpd1* were induced in the jejunum but repressed in the liver, indicating TCDD-mediated disruption of fatty acid synthesis and choline metabolism may involve tissue-specific responses. Notably, immune-related common DEGs including MHC class II genes (*H2-Aa*, *H2-Ab1*, *H2-DMb1*, *Cd74*) were exclusively repressed in the jejunum but induced in the liver. All 6 immune-related common DEGs lack pDREs, further supporting the notion that these gene expression changes are attributed to changes in immune cell populations.

Female mouse livers exhibited dose-dependent changes in fat accumulation and immune cell infiltration (Figure 6). H&E staining revealed minimal centriacinar microvesicular vacuolization at 3 μg/kg TCDD, characteristic of hepatic steatosis, whereas 10 μg/kg TCDD elicited mild to moderate microvesicular vacuolization and mild inflammation, indicating progression to steatohepatitis. At 30 μg/kg TCDD, substantial micro- and macrovesicular vacuolization was observed in the centriacinar,

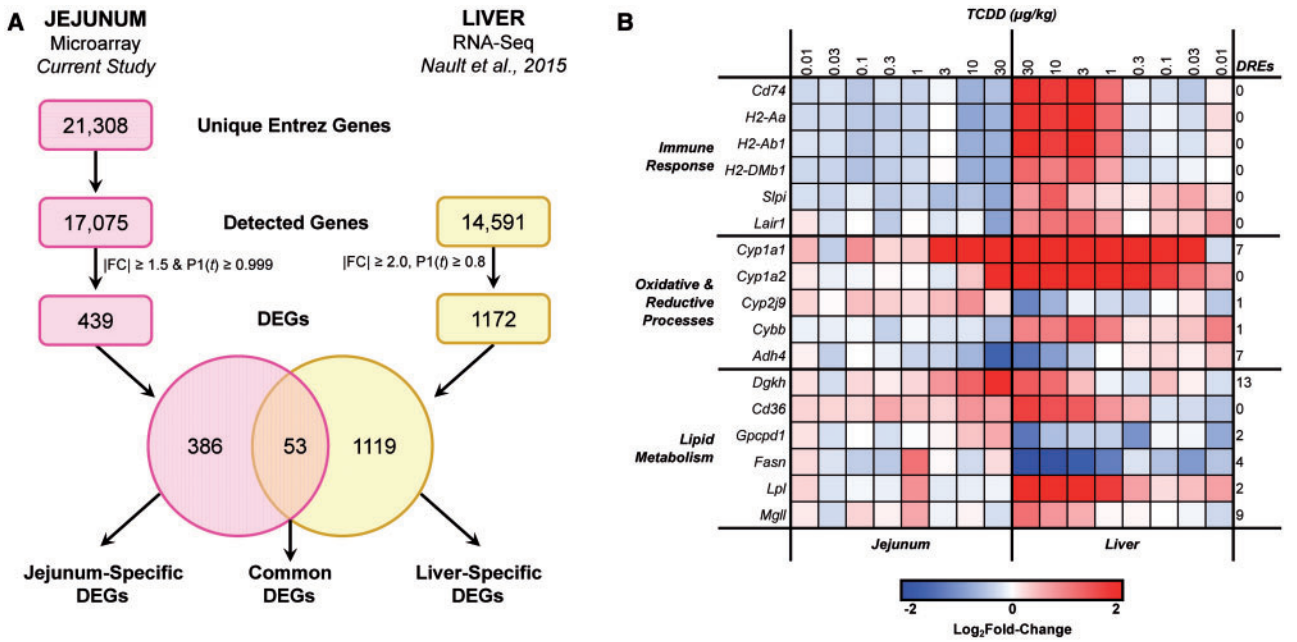

FIG. 5. Comparison of differential gene expression between the jejunal epithelium and liver of female C57BL/6 mice treated by oral gavage with sesame oil vehicle or 0.01–30 µg/kg TCDD every 4 days for 28 days. A, Venn diagram of jejunal and hepatic differentially expressed genes (DEGs), identifying 53 DEGs common to both tissues. B, Heat map of common DEGs associated with immune response, oxidative and reductive processes, and lipid metabolism. The number of pDREs (MS ≥ 0.8473) is indicated in the last column on the right.

midzonal, and periportal regions, accompanied by moderate inflammation and perivenular collagen deposition indicative of modest fibrosis.

ORO staining identified neutral lipid accumulation at 3, 10, and 30 µg/kg TCDD. QuHAnT analysis of digital ORO images confirmed dose-dependent lipid accumulation, with increases of 21- and 67-fold at 10 and 30 µg/kg, respectively. Although vacuole size exhibited a normal distribution, QuHAnT distinguished lipid vacuole size based on published criteria (Zaitoun *et al.*, 2001) with micro ($< 176\ \mu m^2$) vacuole counts increasing 11- and 18-fold at 10 and 30 µg/kg TCDD, respectively, and macro ($\geq 176\ \mu m^2$) vacuole counts increasing 580- and 5092-fold at 10 and 30 µg/kg TCDD, respectively, confirming a transition from micro- to macrovesicular steatosis, consistent with H&E staining. F4/80 labeling indicated inflammatory foci consisted primarily of mature macrophages. Ym1 labeling increased 5.0-, 2.9- (not significant), and 3.0-fold at 3, 10, and 30 µg/kg, respectively, suggesting a polarized M2 macrophage phenotype. Increases in both F4/80 and Ym1 labeling suggest hepatic macrophage infiltration. In contrast, MBP labeling was not affected by TCDD, suggesting eosinophils are not a component of TCDD-mediated hepatic immune cell infiltration (data not shown).

DISCUSSION

Hepatic homeostasis is directly affected by the composition of intestinal contents as the liver receives blood from the intestine through the portal vein, and therefore the gut–liver axis affects NAFLD development (Fukui, 2015; Konrad and Wueest, 2014). Previous studies have shown that dietary fat rather than *de novo* synthesis is a primary lipid source for TCDD-elicited hepatic steatosis (Angrish *et al.*, 2012, 2013). We examined jejunal epithelial gene expression changes in order to investigate intestine–liver interactions in TCDD-elicited steatohepatitis, given the jejunum is the intestinal segment predominantly responsible for dietary lipid absorption (Booth *et al.*, 1961). Jejunal differential gene expression was associated with lipolysis, fatty acid/cholesterol absorption and transport, the Kennedy pathway, and retinol metabolism, suggesting TCDD-elicited alterations in lipid processing which are consistent with hepatic fat accumulation. Furthermore, several MHC class II genes exclusively expressed by professional antigen-presenting cells were repressed, coincident with macrophage and DC decreases in the intestinal lamina propria. The reciprocal increase in hepatic MHC class II expression and infiltration of macrophages lead us to speculate that immune cells may be migrating from the intestine to the liver.

Dose-dependent TCDD-mediated differential expression of lipid metabolism and transport genes in the jejunal epithelium is consistent with increased hepatic lipid accumulation. Genes involved in digestion of dietary fat and protein, including lipases (eg, *Pnlip*, *Clps*, *Mgll*) and proteases (eg, *Cpa2*, *Prss2*, *Cpb1*, *Ctrc*, *Cela1*), respectively, were among the most induced genes, suggesting that TCDD enhances dietary nutrient digestion. *Cd36* induction and cystic fibrosis transmembrane conductance regulator (*Cftr*) repression may promote fatty acid absorption, packaging, and clearance of intestinal lipoproteins as enterocytes from CD36-null mice exhibit reduced fatty acid uptake and chylomicron secretion (Drover *et al.*, 2005; Nassir *et al.*, 2007), whereas Caco-2/15 cells deficient in CFTR exhibit enhanced fatty acid uptake and transport (Mailhot *et al.*, 2009, 2010). Furthermore, TCDD may alter the fatty acid composition of intestinal lipids through induction of stearoyl-CoA desaturase 2 (*Scd2*), consistent with an increase in the desaturation index (18:1n9/18:0) in TCDD-treated mice (Angrish *et al.*, 2013). Repression of cholesterol uptake (*Npc1l1*, *Abca1*) and trafficking (*Stard4*) genes suggests impaired absorption of dietary cholesterol, congruous with decreased serum cholesterol levels. Previous studies report increased cholesterol esters in the liver

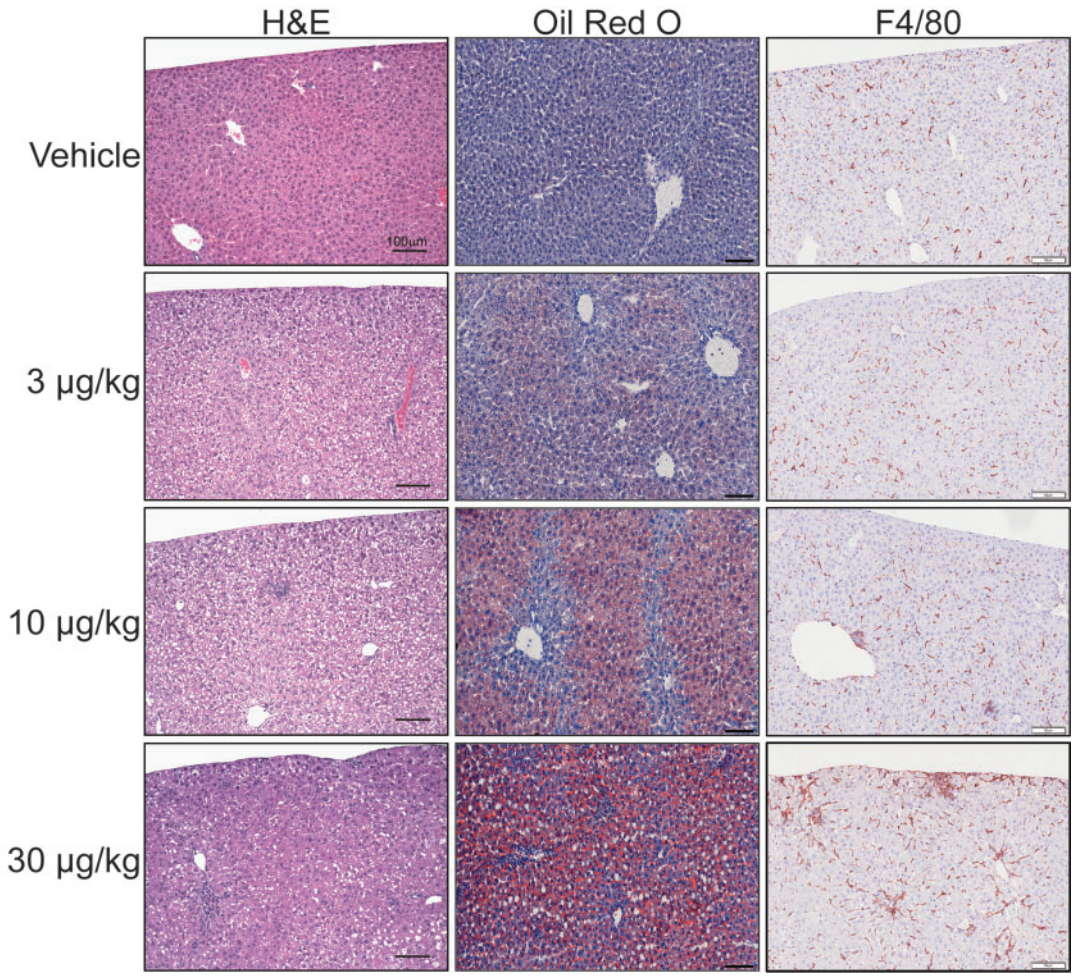

FIG. 6. Representative images of hepatic lesions in female mice treated by oral gavage with sesame oil vehicle or 3–30 µg/kg TCDD every 4 days for 28 days. Livers were stained with hematoxylin and eosin (H&E) (left), Oil Red O (center), or anti-mouse F4/80 antibody (right). Scale bar represents 100 µm.

of TCDD-treated mice, likely due to increased hepatic uptake of high density lipoprotein and low density lipoprotein remnants, rather than *de novo* cholesterol biosynthesis (Angrish *et al.*, 2013; Boverhof *et al.*, 2005; Tanos *et al.*, 2012), further depleting serum cholesterol levels.

Downregulation of the PC branch of the Kennedy pathway suggests TCDD represses *de novo* synthesis using choline and DAG. Since PC is the predominant phospholipid in the chylomicron envelope, insufficient dietary or biliary PC reduces TAG clearance from the intestinal mucosa resulting in dietary fat retention in jejunal enterocytes (O'Doherty *et al.*, 1973). However, jejunal epithelium H&E analysis did not reveal vacuolization within the enterocytes, suggesting dietary fat clearance was not affected by TCDD. Alternatively, negative feedback on the Kennedy pathway may have been initiated in response to sufficient PC stores from alternative sources such as phosphatidylethanolamine methylation.

TCDD is reported to elicit dose-dependent decreases in hepatic vitamin A levels. The induction of *Cd36* and *Scarb1*, the transporters primarily responsible for provitamin A carotenoid uptake (Reboul, 2013), suggests hepatic vitamin A depletion is not due to insufficient dietary β-carotene absorption (Fletcher *et al.*, 2001; Hakansson *et al.*, 1991). Alternatively, retinol dehydrogenase (*Rdh7* and *Rdh16*) and alcohol dehydrogenase (*Adh4*) repression may decrease retinal to retinol conversion and thus retinyl ester synthesis, potentially impairing chylomicron packaging and hepatic delivery. Interestingly, previous studies have shown that CYP1B1 is involved in the oxidation of retinol to retinal (Choudhary *et al.*, 2004), and thus TCDD-mediated induction of *Cyp1b1* (1.4-fold) may further impede the synthesis of retinyl esters. Furthermore, hepatic vitamin A deficiency in C57BL/6JF1 mice leads to fatty liver, likely as a result of PPARα-mediated repression of fatty acid beta oxidation (Kang *et al.*, 2007). Therefore, decreased hepatic vitamin A levels may also be a contributing factor in TCDD-mediated hepatic steatosis.

The intestinal lamina propria is well equipped with mononuclear phagocytes, including both DCs and macrophages, which are responsible for sampling potentially harmful antigens in the intestinal lumen. All subsets of intestinal lamina propria DCs are constitutively migratory in nature (Cerovic *et al.*, 2013). In contrast, intestinal resident macrophages have historically been reported to be non-migratory, although $CX3CR1^{high}$ macrophages are capable of trafficking toward mesenteric lymph nodes under conditions of dysbiosis (Diehl *et al.*, 2013). Interestingly, AhR activation modifies the gut microbiota of mice (Zhang *et al.*, 2015), potentially creating a dysbiotic state inducing migratory behavior in macrophages.

We demonstrate that TCDD decreases macrophages and DC subtypes in the intestinal lamina propria with concurrent increases in hepatic macrophages. Reciprocal changes in these

immune cell populations may be driven by several underlying mechanisms. First, intestinal macrophages and DCs themselves may migrate from the intestine to the liver. The liver is continuously supplied with blood from the intestine through the portal vein, providing a direct link between the 2 tissues. During conditions of intestinal inflammation such as inflammatory bowel disease, blood monocytes are known to migrate from systemic circulation into the lamina propria (Grimm *et al.*, 1995), suggesting emigration of immune cells from the lamina propria into the portal vein is possible. Second, macrophages and DCs from the lamina propria may migrate into mesenteric lymph nodes following exposure to a foreign antigen such as lipopolysaccharide, which would initiate differentiation of naïve T cells into regulatory or effector cells. Activated T cells secrete various inflammatory chemokines that can be transferred to the liver via the portal vein and initiate macrophage infiltration. Pathogenic CD4 Th1 T cell clones are reported to recruit and activate macrophages through CCL1, CCL3 and CCL5 secretion (Cantor and Haskins, 2007). Regardless of the mechanism, several chemokines and chemokine receptors involved in macrophage recruitment, including *Ccr1, Ccr5, Ccl5,* and *Cx3cr1*, were induced 2.1- to 4.8-fold in the liver, suggesting involvement of chemokine signaling in hepatic macrophage infiltration. Other studies have also reported a link between the intestinal immune system and hepatic immune cell infiltration. For example, intestinal inflammation is associated with infiltration of mononuclear cells into the liver, accompanied by emergence of macrophages and classical DCs, which predispose the liver to inflammation (Mikami *et al.*, 2014).

Collectively, we demonstrate that TCDD elicits transcriptome and immune cell population changes in the jejunum that would be expected to promote hepatic lipid accumulation, macrophage infiltration, and the progression to steatohepatitis. Although levels of TCDD and related dioxin-like compounds in the environment are decreasing, the accumulative exposure to all potential AhR ligands, such as polyaromatic hydrocarbons, flame retardants, and natural products, may be increasing and inducing conditions favorable to MetS and NAFLD development (Denison and Nagy, 2003; Lim *et al.*, 2008; Wiseman *et al.*, 2011). Furthermore, it is likely that TCDD-elicited changes in other intestinal segments also contribute to the development of hepatic steatosis and its progression to steatohepatitis.

FUNDING

This work was supported by the National Institute of Environmental Health Sciences Superfund Basic Research Program (NIEHS SBRP P42ES04911) to N.E.K. and T.R.Z. T.R.Z. is partially supported by AgBioResearch at Michigan State University. K.A.F. is supported by the Canadian Institutes of Health Research (CIHR) Doctoral Foreign Study Award (DFS-140386). R.N. is supported by the MSU Barnett Rosenberg Endowed Assistantship.

SUPPLEMENTARY DATA

Supplementary data are available online at http://toxsci.oxfordjournals.org/.

REFERENCES

Alberti, K. G., Eckel, R. H., Grundy, S. M., Zimmet, P. Z., Cleeman, J. I., Donato, K. A., Fruchart, J. C., James, W. P., Loria, C. M., and Smith, S. C., Jr. (2009). Harmonizing the metabolic syndrome: A joint interim statement of the International Diabetes Federation Task Force on Epidemiology and Prevention; National Heart, Lung, and Blood Institute; American Heart Association; World Heart Federation; International Atherosclerosis Society; and International Association for the Study of Obesity. *Circulation* **120**, 1640–1645.

Angrish, M., Mets, B., Jones, A., and Zacharewski, T. (2012). Dietary Fat is a Lipid Source in 2,3,7,8-Tetrachlorodibenzo-para-dioxin (TCDD)-Elicited Hepatic Steatosis in C57BL/6 Mice. *Toxicol. Sci* **128**, 377–386.

Angrish, M. M., Dominici, C. Y., and Zacharewski, T. R. (2013). TCDD-elicited effects on liver, serum, and adipose lipid composition in C57BL/6 mice. *Toxicol. Sci.* **131**, 108–115.

Beischlag, T. V., Luis Morales, J., Hollingshead, B. D., and Perdew, G. H. (2008). The aryl hydrocarbon receptor complex and the control of gene expression. *Crit. Rev. Eukaryot. Gene Expr.* **18**, 207–250.

Bhat, V. S., Hester, S. D., Nesnow, S., and Eastmond, D. A. (2013). Concordance of transcriptional and apical benchmark dose levels for conazole-induced liver effects in mice. *Toxicol. Sci.* **136**, 205–215.

Birnbaum, L. S. (1986). Distribution and excretion of 2,3,7,8-tetrachlorodibenzo-p-dioxin in congenic strains of mice which differ at the Ah locus. *Drug Metab. Dispos.* **14**, 34–40.

Booth, C. C., Read, A. E., and Jones, E. (1961). Studies on the site of fat absorption: 1. The sites of absorption of increasing doses of I-labelled triolein in the rat. *Gut* **2**, 23–31.

Boverhof, D. R., Burgoon, L. D., Tashiro, C., Chittim, B., Harkema, J. R., Jump, D. B., and Zacharewski, T. R. (2005). Temporal and dose-dependent hepatic gene expression patterns in mice provide new insights into TCDD-Mediated hepatotoxicity. *Toxicol. Sci.* **85**, 1048–1063.

Burgoon, L. D., Eckel-Passow, J. E., Gennings, C., Boverhof, D. R., Burt, J. W., Fong, C. J., and Zacharewski, T. R. (2005). Protocols for the assurance of microarray data quality and process control. *Nucleic Acids Res.* **33**, e172.

Burgoon, L. D., and Zacharewski, T. R. (2008). Automated quantitative dose-response modeling and point of departure determination for large toxicogenomic and high-throughput screening data sets. *Toxicol. Sci.* **104**, 412–418.

Cantor, J., and Haskins, K. (2007). Recruitment and activation of macrophages by pathogenic CD4 T cells in type 1 diabetes: Evidence for involvement of CCR8 and CCL1. *J. Immunol.* **179**, 5760–5767.

Casals-Casas, C., and Desvergne, B. (2011). Endocrine disruptors: From endocrine to metabolic disruption. *Annu. Rev. Physiol.* **73**, 135–162.

Cerovic, V., Houston, S. A., Scott, C. L., Aumeunier, A., Yrlid, U., Mowat, A. M., and Milling, S. W. (2013). Intestinal CD103(-) dendritic cells migrate in lymph and prime effector T cells. *Mucosal Immunol.* **6**, 104–113.

Chen, J. Q., Brown, T. R., and Russo, J. (2009). Regulation of energy metabolism pathways by estrogens and estrogenic chemicals and potential implications in obesity associated with increased exposure to endocrine disruptors. *Biochim. Biophys. Acta.* **1793**, 1128–1143.

Choudhary, D., Jansson, I., Stoilov, I., Sarfarazi, M., and Schenkman, J. B. (2004). Metabolism of retinoids and arachidonic acid by human and mouse cytochrome P450 1b1. *Drug Metab. Dispos.* **32**, 840–847.

Cimafranca, M. A., Hanlon, P. R., and Jefcoate, C. R. (2004). TCDD administration after the pro-adipogenic differentiation

stimulus inhibits PPARgamma through a MEK-dependent process but less effectively suppresses adipogenesis. *Toxicol. Appl. Pharmacol.* **196**, 156–168.

Cohn, J. S., Kamili, A., Wat, E., Chung, R. W., and Tandy, S. (2010). Dietary phospholipids and intestinal cholesterol absorption. *Nutrients* **2**, 116–127.

Denison, M. S., and Nagy, S. R. (2003). Activation of the aryl hydrocarbon receptor by structurally diverse exogenous and endogenous chemicals. *Annu. Rev. Pharmacol. Toxicol.* **43**, 309–334.

Denison, M. S., Pandini, A., Nagy, S. R., Baldwin, E. P., and Bonati, L. (2002). Ligand binding and activation of the Ah receptor. *Chem. Biol. Interact.* **141**, 3–24.

Denison, M. S., Soshilov, A. A., He, G., DeGroot, D. E., and Zhao, B. (2011). Exactly the same but different: Promiscuity and diversity in the molecular mechanisms of action of the aryl hydrocarbon (dioxin) receptor. *Toxicol. Sci.* **124**, 1–22.

Dere, E., Forgacs, A. L., Zacharewski, T. R., and Burgoon, L. D. (2011a). Genome-wide computational analysis of dioxin response element location and distribution in the human, mouse, and rat genomes. *Chem. Res. Toxicol.* **24**, 494–504.

Dere, E., Lo, R., Celius, T., Matthews, J., and Zacharewski, T. R. (2011b). Integration of genome-wide computation DRE search, AhR ChIP-chip and gene expression analyses of TCDD-elicited responses in the mouse liver. *BMC Genomics* **12**, 365.

Diehl, G. E., Longman, R. S., Zhang, J. X., Breart, B., Galan, C., Cuesta, A., Schwab, S. R., and Littman, D. R. (2013). Microbiota restricts trafficking of bacteria to mesenteric lymph nodes by CX(3)CR1(hi) cells. *Nature* **494**, 116–120.

Doe, W. F. (1989). The intestinal immune system. *Gut* **30**, 1679–1685.

Drover, V. A., Ajmal, M., Nassir, F., Davidson, N. O., Nauli, A. M., Sahoo, D., Tso, P., and Abumrad, N. A. (2005). CD36 deficiency impairs intestinal lipid secretion and clearance of chylomicrons from the blood. *J. Clin. Invest.* **115**, 1290–1297.

Eckel, J. E., Gennings, C., Chinchilli, V. M., Burgoon, L. D., and Zacharewski, T. R. (2004). Empirical Bayes gene screening tool for time-course or dose-response microarray data. *J. Biopharm. Stat.* **14**, 647–670.

Eckel, J. E., Gennings, C., Therneau, T. M., Burgoon, L. D., Boverhof, D. R., and Zacharewski, T. R. (2005). Normalization of two-channel microarray experiments: A semiparametric approach. *Bioinformatics* **21**, 1078–1083.

Fletcher, N., Hanberg, A., and Hakansson, H. (2001). Hepatic vitamin a depletion is a sensitive marker of 2,3,7,8-tetrachlorodibenzo-p-dioxin (TCDD) exposure in four rodent species. *Toxicol. Sci.* **62**, 166–175.

Ford, E. S., Li, C., and Zhao, G. (2010). Prevalence and correlates of metabolic syndrome based on a harmonious definition among adults in the US. *J. Diabetes* **2**, 180–193.

Forgacs, A. L., Kent, M. N., Makley, M. K., Mets, B., DelRaso, N., Jahns, G. L., Burgoon, L. D., Zacharewski, T. R., and Reo, N. V. (2012). Comparative metabolomic and genomic analyses of TCDD-elicited metabolic disruption in mouse and rat liver. *Toxicol. Sci.* **125**, 41–55.

Fukui, H. (2015). Gut-liver axis in liver cirrhosis: How to manage leaky gut and endotoxemia. *World J. Hepatol.* **7**, 425–442.

Gasiewicz, T. A., Geiger, L. E., Rucci, G., and Neal, R. A. (1983). Distribution, excretion, and metabolism of 2,3,7,8-tetrachlorodibenzo-p-dioxin in C57BL/6J, DBA/2J, and B6D2F1/J mice. *Drug Metab. Dispos.* **11**, 397–403.

Geem, D., Medina-Contreras, O., Kim, W., Huang, C. S., and Denning, T. L. (2012). Isolation and characterization of dendritic cells and macrophages from the mouse intestine. *J. Vis. Exp.* e4040.

Grimm, M. C., Pullman, W. E., Bennett, G. M., Sullivan, P. J., Pavli, P., and Doe, W. F. (1995). Direct evidence of monocyte recruitment to inflammatory bowel disease mucosa. *J. Gastroenterol. Hepatol.* **10**, 387–395.

Grun, F., and Blumberg, B. (2009). Endocrine disrupters as obesogens. *Mol. Cell Endocrinol.* **304**, 19–29.

Grundy, S. M. (2008). Metabolic syndrome pandemic. *Arterioscler. Thromb. Vasc. Biol.* **28**, 629–636.

Hakansson, H., Johansson, L., Manzoor, E., and Ahlborg, U. G. (1991). Effects of 2,3,7,8-tetrachlorodibenzo-p-dioxin (TCDD) on the vitamin A status of Hartley guinea pigs, Sprague-Dawley rats, C57Bl/6 mice, DBA/2 mice, and Golden Syrian hamsters. *J. Nutr. Sci. Vitaminol.* **37**, 117–138.

Hamilton, J. A. (1998). Fatty acid transport: Difficult or easy? *J. Lipid Res.* **39**, 467–481.

Hankinson, O. (1995). The aryl hydrocarbon receptor complex. *Annu. Rev. Pharmacol. Toxicol.* **35**, 307–340.

Huang, G., and Elferink, C. J. (2012). A novel nonconsensus xenobiotic response element capable of mediating aryl hydrocarbon receptor-dependent gene expression. *Mol. Pharmacol.* **81**, 338–347.

Kang, H. W., Bhimidi, G. R., Odom, D. P., Brun, P. J., Fernandez, M. L., and McGrane, M. M. (2007). Altered lipid catabolism in the vitamin A deficient liver. *Mol. Cell Endocrinol.* **271**, 18–27.

Konrad, D., and Wueest, S. (2014). The gut-adipose-liver axis in the metabolic syndrome. *Physiology* **29**, 304–313.

Kopec, A. K., Boverhof, D. R., Nault, R., Harkema, J. R., Tashiro, C., Potter, D., Sharratt, B., Chittim, B., and Zacharewski, T. R. (2013). Toxicogenomic evaluation of long-term hepatic effects of TCDD in immature, ovariectomized C57BL/6 mice. *Toxicol. Sci.* **135**, 465–475.

Kopec, A. K., Burgoon, L. D., Ibrahim-Aibo, D., Burg, A. R., Lee, A. W., Tashiro, C., Potter, D., Sharratt, B., Harkema, J. R., Rowlands, J. C., *et al.* (2010a). Automated dose-response analysis and comparative toxicogenomic evaluation of the hepatic effects elicited by TCDD, TCDF, and PCB126 in C57BL/6 mice. *Toxicol. Sci.* **118**, 286–297.

Kopec, A. K., Burgoon, L. D., Ibrahim-Aibo, D., Mets, B. D., Tashiro, C., Potter, D., Sharratt, B., Harkema, J. R., and Zacharewski, T. R. (2010b). PCB153-elicited hepatic responses in the immature, ovariectomized C57BL/6 mice: Comparative toxicogenomic effects of dioxin and non-dioxin-like ligands. *Toxicol. Appl. Pharmacol.* **243**, 359–371.

Kopec, A. K., D'Souza, M. L., Mets, B. D., Burgoon, L. D., Reese, S. E., Archer, K. J., Potter, D., Tashiro, C., Sharratt, B., Harkema, J. R., *et al.* (2011). Non-additive hepatic gene expression elicited by 2,3,7,8-tetrachlorodibenzo-p-dioxin (TCDD) and 2,2',4,4',5,5'-hexachlorobiphenyl (PCB153) co-treatment in C57BL/6 mice. *Toxicol. Appl. Pharmacol.* **256**, 154–167.

Lee, J. H., Wada, T., Febbraio, M., He, J., Matsubara, T., Lee, M. J., Gonzalez, F. J., and Xie, W. (2010). A novel role for the dioxin receptor in fatty acid metabolism and hepatic steatosis. *Gastroenterology* **139**, 653–663.

Leung, H. W., Wendling, J. M., Orth, R., Hileman, F., and Paustenbach, D. J. (1990). Relative distribution of 2,3,7,8-tetrachlorodibenzo-p-dioxin in human hepatic and adipose tissues. *Toxicol. Lett.* **50**, 275–282.

Lim, J. S., Lee, D. H., and Jacobs, D. R., Jr. (2008). Association of brominated flame retardants with diabetes and metabolic syndrome in the U.S. population, 2003-2004. *Diabetes Care* **31**, 1802–1807.

Mailhot, G., Rabasa-Lhoret, R., Moreau, A., Berthiaume, Y., and Levy, E. (2010). CFTR depletion results in changes in fatty acid composition and promotes lipogenesis in intestinal Caco 2/15 cells. *PLoS One* **5**, e10446.

Mailhot, G., Ravid, Z., Barchi, S., Moreau, A., Rabasa-Lhoret, R., and Levy, E. (2009). CFTR knockdown stimulates lipid synthesis and transport in intestinal Caco-2/15 cells. *Am. J. Physiol. Gastrointest. Liver Physiol.* **297**, G1239–G1249.

Michalek, J. E., Pirkle, J. L., Caudill, S. P., Tripathi, R. C., Patterson, D. G., Jr., and Needham, L. L. (1996). Pharmacokinetics of TCDD in veterans of Operation Ranch Hand: 10-year follow-up. *J. Toxicol. Environ. Health.* **47**, 209–220.

Mikami, Y., Mizuno, S., Nakamoto, N., Hayashi, A., Sujino, T., Sato, T., Kamada, N., Matsuoka, K., Hisamatsu, T., Ebinuma, H., *et al.* (2014). Macrophages and dendritic cells emerge in the liver during intestinal inflammation and predispose the liver to inflammation. *PLoS One* **9**, e84619.

Nassir, F., Wilson, B., Han, X., Gross, R. W., and Abumrad, N. A. (2007). CD36 is important for fatty acid and cholesterol uptake by the proximal but not distal intestine. *J. Biol. Chem.* **282**, 19493–19501.

Nault, R., Colbry, D., Brandenberger, C., Harkema, J. R., and Zacharewski, T. R. (2015a). Development of a computational high-throughput tool for the quantitative examination of dose-dependent histological features. *Toxicol. Pathol.* **43**, 366–375.

Nault, R., Fader, K. A., and Zacharewski, T. (2015b). RNA-Seq versus oligonucleotide array assessment of dose-dependent TCDD-elicited hepatic gene expression in mice. *BMC Genomics* **16**, 373.

O'Doherty, P. J., Kakis, G., and Kuksis, A. (1973). Role of luminal lecithin in intestinal fat absorption. *Lipids* **8**, 249–255.

Olufadi, R., and Byrne, C. D. (2008). Clinical and laboratory diagnosis of the metabolic syndrome. *J. Clin. Pathol.* **61**, 697–706.

Paschos, P., and Paletas, K. (2009). Non alcoholic fatty liver disease and metabolic syndrome. *Hippokratia* **13**, 9–19.

Pierre, S., Chevallier, A., Teixeira-Clerc, F., Ambolet-Camoit, A., Bui, L. C., Bats, A. S., Fournet, J. C., Fernandez-Salguero, P., Aggerbeck, M., Lotersztajn, S., *et al.* (2014). Aryl hydrocarbon receptor-dependent induction of liver fibrosis by dioxin. *Toxicol. Sci.* **137**, 114–124.

Pirkle, J. L., Wolfe, W. H., Patterson, D. G., Needham, L. L., Michalek, J. E., Miner, J. C., Peterson, M. R., and Phillips, D. L. (1989). Estimates of the half-life of 2,3,7,8-tetrachlorodibenzo-p-dioxin in Vietnam Veterans of Operation Ranch Hand. *J. Toxicol. Environ. Health* **27**, 165–171.

Reboul, E. (2013). Absorption of vitamin A and carotenoids by the enterocyte: Focus on transport proteins. *Nutrients* **5**, 3563–3581.

Sorg, O., Zennegg, M., Schmid, P., Fedosyuk, R., Valikhnovskyi, R., Gaide, O., Kniazevych, V., and Saurat, J. H. (2009). 2,3,7,8-tetrachlorodibenzo-p-dioxin (TCDD) poisoning in Victor Yushchenko: Identification and measurement of TCDD metabolites. *Lancet* **374**, 1179–1185.

Tanos, R., Patel, R. D., Murray, I. A., Smith, P. B., Patterson, A. D., and Perdew, G. H. (2012). Aryl hydrocarbon receptor regulates the cholesterol biosynthetic pathway in a dioxin response element-independent manner. *Hepatology* **55**, 1994–2004.

Taylor, K. W., Novak, R. F., Anderson, H. A., Birnbaum, L. S., Blystone, C., Devito, M., Jacobs, D., Kohrle, J., Lee, D. H., Rylander, L., *et al.* (2013). Evaluation of the Association between Persistent Organic Pollutants (POPs) and Diabetes in Epidemiological Studies: A National Toxicology Program Workshop Review. *Environ Health Perspect.* **121**, 774–783.

Tomasello, E., and Bedoui, S. (2013). Intestinal innate immune cells in gut homeostasis and immunosurveillance. *Immunol. Cell Biol.* **91**, 201–203.

Trauner, M., Arrese, M., and Wagner, M. (2010). Fatty liver and lipotoxicity. *Biochim. Biophys. Acta* **1801**, 299–310.

Vanni, E., Bugianesi, E., Kotronen, A., De Minicis, S., Yki-Jarvinen, H., and Svegliati-Baroni, G. (2010). From the metabolic syndrome to NAFLD or vice versa? *Dig. Liver Dis.* **42**, 320–330.

Wiseman, S. B., Wan, Y., Chang, H., Zhang, X., Hecker, M., Jones, P. D., and Giesy, J. P. (2011). Polybrominated diphenyl ethers and their hydroxylated/methoxylated analogs: Environmental sources, metabolic relationships, and relative toxicities. *Mar. Pollut. Bull* **63**, 179–188.

Wolfe, W. H., Michalek, J. E., Miner, J. C., Pirkle, J. L., Caudill, S. P., Patterson, D. G., Jr., and Needham, L. L. (1994). Determinants of TCDD half-life in veterans of operation ranch hand. *J. Toxicol. Environ. Health* **41**, 481–488.

Yang, L., Allen, B. C., and Thomas, R. S. (2007). BMDExpress: A software tool for the benchmark dose analyses of genomic data. *BMC Genomics* **8**, 387.

Zaitoun, A. M., Al Mardini, H., Awad, S., Ukabam, S., Makadisi, S., and Record, C. O. (2001). Quantitative assessment of fibrosis and steatosis in liver biopsies from patients with chronic hepatitis C. *J. Clin. Pathol.* **54**, 461–465.

Zhang, L., Nichols, R. G., Correll, J., Murray, I. A., Tanaka, N., Smith, P., Hubbard, T. D., Sebastian, A., Albert, I., Hatzakis, E., *et al.* (2015). Persistent Organic Pollutants Modify Gut Microbiota-Host Metabolic Homeostasis in Mice Through Aryl Hydrocarbon Receptor Activation. *Environ Health Perspect.* **123**, 679–688.